Advanced Composite Materials
Publication details, including instructions for authors and subscription information:
http://www.tandfonline.com/loi/tacm20

Numerical validation of split Hopkinson pressure bar technique for evaluating tensile mechanical properties of CFRP laminates

Kazuhiro Suga [a], Kazuya Okamoto [b], Kenji Takagi [b], Hayato Nakatani [a], Shinji Ogihara [a] & Masanori Kikuchi [a]

[a] Faculty of Science and Technology, Department of Mechanical Engineering, Tokyo University of Science, 2641 Yamazaki, Noda, Chiba, 278-8510, Japan

[b] Department of Mechanical Engineering, Graduate School of Science and Technology, Tokyo University of Science, 2641 Yamazaki, Noda, Chiba, 278-8510, Japan

Version of record first published: 11 Sep 2012.

To cite this article: Kazuhiro Suga , Kazuya Okamoto , Kenji Takagi , Hayato Nakatani , Shinji Ogihara & Masanori Kikuchi (2012): Numerical validation of split Hopkinson pressure bar technique for evaluating tensile mechanical properties of CFRP laminates, Advanced Composite Materials, 21:3, 221-232

To link to this article: http://dx.doi.org/10.1080/09243046.2012.723331

Advanced Composite Materials
Vol. 21, No. 3, June 2012, 221–232

Numerical validation of split Hopkinson pressure bar technique for evaluating tensile mechanical properties of CFRP laminates

Kazuhiro Suga[a]*, Kazuya Okamoto[b], Kenji Takagi[b], Hayato Nakatani[a], Shinji Ogihara[a] and Masanori Kikuchi[a]

[a]*Faculty of Science and Technology, Department of Mechanical Engineering, Tokyo University of Science, 2641 Yamazaki, Noda, Chiba 278-8510, Japan;* [b]*Department of Mechanical Engineering, Graduate School of Science and Technology, Tokyo University of Science, 2641 Yamazaki, Noda, Chiba 278-8510, Japan*

(*Received 30 October 2011; final version received 13 June 2012*)

The present study proposes a simple numerical simulation technique for the split Hopkinson pressure bar (SHPB) and then investigates the experimental conditions for composite materials in a tensile-loading SHPB. The following issues were investigated through experiment and numerical simulation: (i) the effects of the cross section and acoustic mismatch between the jig with a slit and screw and the input/output bars on the loading condition and (ii) the effects of the duration time of the applied load and the acoustic impedance mismatch on the stress–strain curve obtained by SHPB testing. From the numerical simulation results, the following conclusions were found: (i) the proposed jig with a slit and screw can apply an ideal one-dimensional displacement to a specimen and (ii) the material characterization of a composite material by SHPB testing might be possible by optimizing a longer duration time if the acoustic mismatch is greater.

Keywords: split Hopkinson pressure bar; jig; numerical simulation; tensile loading; acoustic impedance mismatch; composite material

1. Introduction

Material characterization of composite materials under dynamic loading is important in the designing of safe and efficient structures. The split Hopkinson pressure bar (SHPB) has been widely used to characterize the dynamic behavior of metal materials. In recent years, the application of the SHPB to composite materials has been a topic of much interest; for example, the behavior of carbon/epoxy composites under dynamic loading was studied in [1–3] and the behavior of glass/epoxy composites was studied in [4]. SHPB testing under tensile loading has also been performed on composite materials [5,6]; however, its effectiveness is examining because the experimental conditions for composite materials are significantly different from the conditions for metal materials.

Composite material specimens are usually obtained in flat plates due to limitations of the fabrication process; it is difficult to form composites into solid cylinders and machine them into screws. Therefore, a special jig is required to join the flat specimens to the input/output bars. In addition, the Young's modulus becomes significantly smaller compared with that of

*Corresponding author. Email: ksuga@rs.noda.tus.ac.jp

ISSN 0924-3046 print/ISSN 1568-5519 online

http://dx.doi.org/10.1080/09243046.2012.723331
http://www.tandfonline.com

the input/output bars when the fiber direction is off-axis to the loading direction. The effects of the special jig and the difference in Young's modulus on the material characterization should be investigated to ensure a reasonable characterization.

The present study investigates the experimental conditions for composite materials in a tensile-loading SHPB. The following issues are investigated through experiment and numerical simulation:

(i) The effects of the cross section and acoustic mismatch between the jig with a slit and screw and the input/output bars on the loading condition.
(ii) The effects of the duration time of the applied load and the acoustic impedance mismatch on the stress–strain curves obtained by SHPB testing.

In addition, in order to resolve the above issues, this study proposes a simple numerical simulation technique for the SHPB.

2. Split Hopkinson pressure bar

This section presents a theoretical overview of the SHPB. In the SHPB, the strain and stress applied to a specimen can be calculated based on one-dimensional stress wave theory. Figure 1 shows the propagation of a stress wave in a specimen that connects the input/output bars. The stress wave propagates from the left side of the figure through the input bar and the strain ε_{i} from the incident wave is measured by gage 1. A portion of the stress wave is reflected at the boundary between the input bar and the specimen and this reflected wave is measured by gage 1 as strain ε_{r}. The transmitted wave propagates through the specimen and is measured by gage 2 as strain ε_t.

Assuming that the load at each end of the specimen is identical, the strain rate $\dot{\varepsilon}_{\mathrm{s}}(t)$, strain $\varepsilon_{\mathrm{s}}(t)$, and stress σ_{s} can be given by:

$$\dot{\varepsilon}_{\mathrm{s}}(t) = \frac{\mathrm{d}\varepsilon_{\mathrm{s}}(t)}{\mathrm{d}t} = \frac{c_{\mathrm{i}}\{\varepsilon_{\mathrm{i}}(t) - \varepsilon_{\mathrm{r}}(t)\} - c_{\mathrm{o}}\varepsilon_{\mathrm{t}}(t)}{l_{\mathrm{s}}} \tag{1}$$

$$\varepsilon_{\mathrm{s}}(t) = \frac{1}{l_{\mathrm{s}}}\int_0^t [c_{\mathrm{i}}\{\varepsilon_{\mathrm{i}}(t) - \varepsilon_{\mathrm{r}}(t)\} - c_{\mathrm{o}}\varepsilon_{\mathrm{t}}(t)]\mathrm{d}t \tag{2}$$

$$\sigma_{\mathrm{s}} = \frac{E_{\mathrm{o}}A_{\mathrm{o}}}{A_{\mathrm{s}}}\varepsilon_{\mathrm{t}}(t) \tag{3}$$

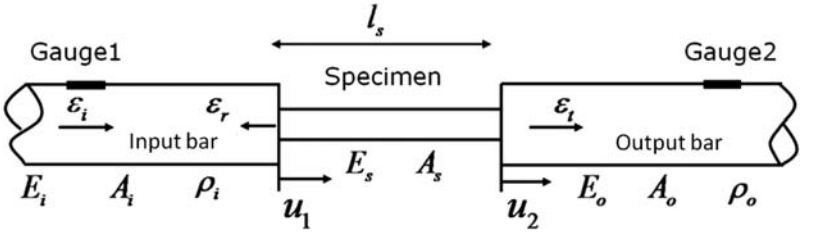

Figure 1. SHPB theory.

where E, c, and A are the elastic modulus, velocity of the longitudinal wave in the medium, and cross-sectional area, respectively. The subscripts i, o, and s denote the input bar, output bar, and specimen, respectively.

3. Experimental apparatus

The apparatus used in this study is shown in Figure 2. It is composed of a 5000 mm long stainless steel input bar 16 mm in diameter, a 750 mm long aluminum (A5056) output bar 8 mm in diameter, and a stainless steel hollow cylinder striker 750 mm in length with a 24/16.2 mm outer/inner diameter. The specimen is set between the input and output bars. The striker is launched by pneumatic pressure retained in the pressure tank and impacts the flange at the end of the input bar resulting in the generation of a stress wave. This wave propagates through the input bar, specimen, and output bar. The launch speed of the striker can be controlled by adjusting the pneumatic pressure.

For measurement of the strain used in Equations (1)–(3), strain gages are installed 1500 mm away from the right end of the input bar and 300 mm away from the left end of the output bar. A strain gage is also installed at the center of the specimen to directly obtain the strain in the specimen. It should be noted that the specimen and the input/output bars are connected via jigs. The specimen is fixed to the jig using an adhesive (Araldite, Huntsman) and the jig is screwed onto the input/output bars to facilitate the changing of specimens. A high-speed camera is used to observe the displacements of the jig and specimen.

4. Numerical simulation

The present study uses a simple numerical simulation technique for the SHPB. This section explains how to create numerical models and perform dynamic finite element analysis.

4.1. Modeling of the SHPB

Figure 3(a) shows a numerical model of the SHPB, which consists of the input and output bars and the specimen. The model is created from the cylinder shown in Figure 3(b), where the diameter of the cylinder is the same as that of the input and output bars, and the length of the cylinder is the same as the total length of the SHPB model shown in Figure 3(a). To create the finite element model, the cylinder is discretized into slices of the same thickness, and then, each slice is discretized into finite elements in the same manner. Finally, we obtain the finite element model shown in Figure 4.

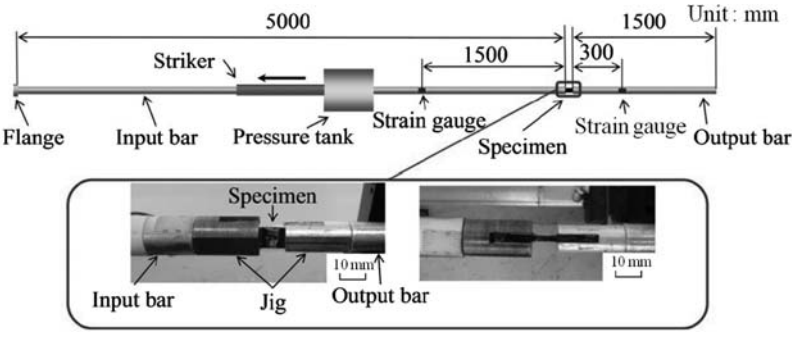

Figure 2. Configuration of the apparatus.

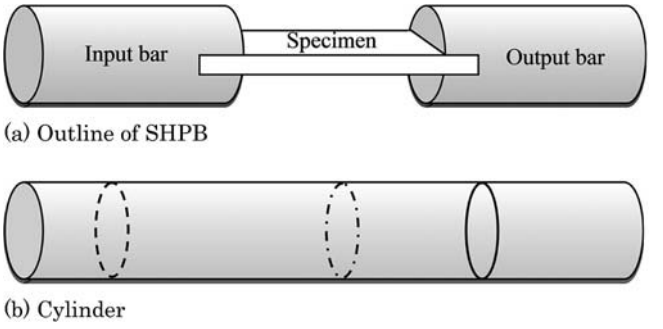

Figure 3. SHPB model.

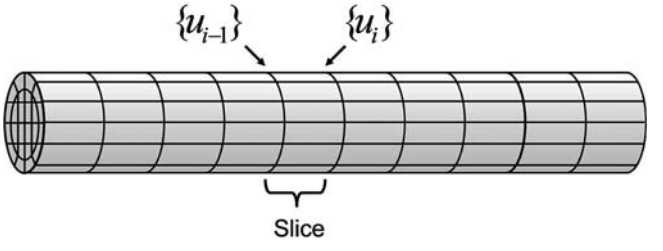

Figure 4. Regular discretization of the cylinder.

To consider the differences in cross section, the present model sets the material constants of the finite elements that do not exist in the SHPB apparatus to zero. Figure 5 shows an example of the material property configuration, where (a) is the cross section of the input bar, (b) is the cross section of the specimen, and (c) is the cross section of the output bar (including part of the specimen). In (a), the material constants of the input bar are used. In (b), the material constants of the specimen are used in the black colored area, and the material constants are set to zero in the gray colored area because there is no material in that area. In (c), the material properties of the specimen are assigned to the area in black and the material properties of the output bar are assigned to the gray area.

4.2. Finite element analysis

In order to easily formulate a finite element equation that simulates the SHPB, two sets of matrix equations are derived. One is for a cylinder discretized in the regular manner shown in Figure 4. Here, the cylinder is assumed to be a homogeneous material. Due to the regular

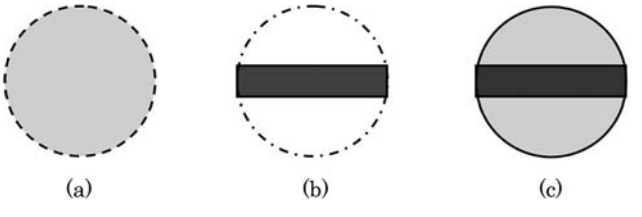

Figure 5. Configurations of the material constants.

discretization and the material assumption, the equation is described with characteristic block tridiagonal matrices [7]:

$$\begin{bmatrix} [A_1] & [A_2] & & & \\ [A_3] & [A_5] & [A_2] & & \\ & \ddots & \ddots & \ddots & \\ & & [A_3] & [A_5] & [A_2] \\ & & & [A_3] & [A_4] \end{bmatrix} \begin{Bmatrix} \{u_0^t\} \\ \{u_1^t\} \\ \vdots \\ \{u_{n-1}^t\} \\ \{u_n^t\} \end{Bmatrix} = \begin{Bmatrix} \{b_0^t\} \\ \{b_1^t\} \\ \vdots \\ \{b_{n-1}^t\} \\ \{b_n^t\} \end{Bmatrix} \tag{4'}$$

where $[A_1]$, $[A_2]$, … , $[A_5]$ (= $[A_4]$ + $[A_1]$) are known small block matrices, $\{u_i^t\}$ is an unknown nodal displacement vector, $\{b_i^t\}$ is a known vector in the ith cross section, t is the time step, and n is the total number of cross sections. Equation (4′) is represented by Equation (4) as follows:

$$[A] \cdot \{u^t\} = \{b^t\} \tag{4}$$

The other matrix equation is for a cylinder that considers the difference in material properties,

$$[\hat{A}]\{\hat{u}^t\} = \left\{\hat{b}^t\right\} \tag{5}$$

where $[\hat{A}]$ is a coefficient matrix, $\{\hat{u}^t\}$ is an unknown displacement vector, and $[\hat{b}^t]$ is a known force vector. The discretizations for Equations (4) and (5) are the same.

The following formulation is used to obtain $\{\hat{u}^t\}$ efficiently with Equations (4) and (5). Subtracting $[\hat{A}]$ $\{\hat{u}^t\}$ from the both sides of Equation (5) and then multiplying by $[\mathrm{A}]^{-1}$ from the left side of the equation yields Equation (6):

$$\{\hat{u}^t\} = \left\{\hat{b}^t\right\} - [D]\{\hat{u}^t\} \tag{6}$$

where $[\hat{b}^t]$ and $[D]$ are defined by the following equations:

$$\left\{\hat{b}\right\}^{t'} = [A]^{-1}\left\{\hat{b}^t\right\} \tag{7}$$

$$[D] = [A]^{-1}\{[\hat{A}] - [A]\} \tag{8}$$

Because Equations (7) and (8) can be calculated efficiently considering the characteristic of the coefficient matrix $[A]$ [7,8], Equation (6) is solved using an iterative method. The recurrence formula of Equation (6) is given by Equation (9):

$$\left\{\hat{u}^{t,(i+1)}\right\} = \left\{\hat{b}'^{t,(i)}\right\} - [D]\left\{\hat{u}''^{(i)}\right\} \tag{9}$$

where i indicates the iteration step. Here, $\{\hat{u}^{t,(i)}\}$ can converge to a true solution if the norm of $[D]$ is less than one. This technique saves memory because we can obtain a solution by solving Equation (6) instead of solving Equation (5) directly [8].

4.3. Verification

In order to verify the proposed simulation technique, we perform a simple experiment and then compare the experimental result with the numerical result. The experiment uses only an input bar and a jig without a slit, as shown in Figure 6, and the input bar and jig are attached with a screw.

Figure 7 shows the dimensions and material property configuration in monochrome color. The material constants are listed in Table 1. This model considers the effects of the screw and the 1 mm gap between the input bar and the jig. Because the materials are discontinuous in the screw part, the constants for the screw part are decreased in the continuum model. Therefore, the screw is modeled by decreasing the material constants to one tenth that of the input and output bars, and the gap is modeled by setting the material constants to zero. In the following simulations, the thickness of each slice is fixed to 1 mm.

A tensile impact load is applied to the left end of the input bar. The loading condition was assumed based on the measured impact load in the experiment. The time history of the load is shown in Figure 8. The solid line shows the measured impact load on the input bar and the dotted line shows the assumed load for the numerical simulation.

Figure 9 compares the obtained time history for the displacement at the left end of the jig for the simulation and experiment. The displacement in the experiment was measured using a high-speed camera. These results are in good agreement, which indicates that the present

Figure 6. Jig with screw.

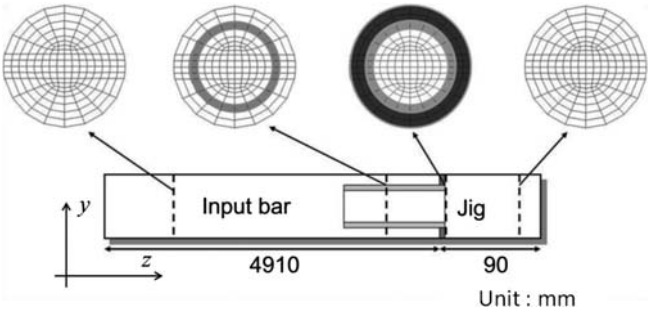

Figure 7. Dimensions of the numerical model and configuration of the material properties.

Table 1. Material constants.

E (GPa)	ν	ρ (kg/m^3)
205	0.25	7800
0	0	0
20.5	0.025	780

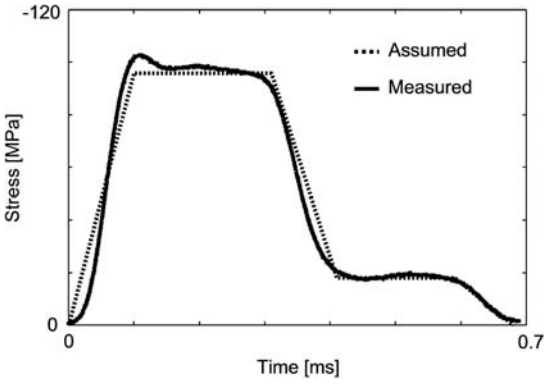

Figure 8. Measured loading by experiment and assumed loading for simulation.

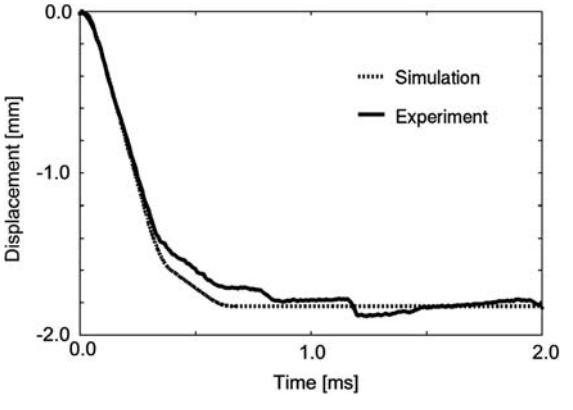

Figure 9. Comparison of displacement between simulation and experiment.

simulation technique is effective at evaluating the dynamic behavior of the input bar and the connected jig with a screw.

5. Investigation

This section investigates: (i) the effect of the jig shape on the loading condition and (ii) the effect of the duration time of the applied load on the stress–strain curves obtained by SHPB testing for several acoustic impedance mismatch conditions. The investigation of (ii) is conducted to determine the experimental conditions that provide reasonable stress–strain curves.

5.1. Effect of jig shape

The composite material specimen is in the form of a plate because of manufacturing constraints. Therefore, the jig has a slit to grip the plate-shaped specimen, as shown in Figure 10. In addition, the jig has a screw to easily connect/disconnect the specimen to/from the input and output bars (i.e. to easily change specimens during the experiment). The effect of the jig shape on the specimen loading was investigated.

Figure 10. Jig having a slit and screw.

The dimensions and mesh discretization are given in Figure 11. The gray elements are used to consider the screw; in these elements, the material properties are lower than those of the base material. The black elements are used to consider the slit, and the material constants are set as zero in the slit area. This simulation considers the input bar and the jig. Figure 12 shows the material property configuration for each different cross section, and their material properties are shown in monochrome colors, which correspond to the properties shown in Table 1. Because the materials are discontinuous in the screw part, the material constants of the screw part are decreased in continuum modeling. We applied the impact loading shown in Figure 13 at the left end of the input bar. A total of 273,856 elements were used in the numerical model.

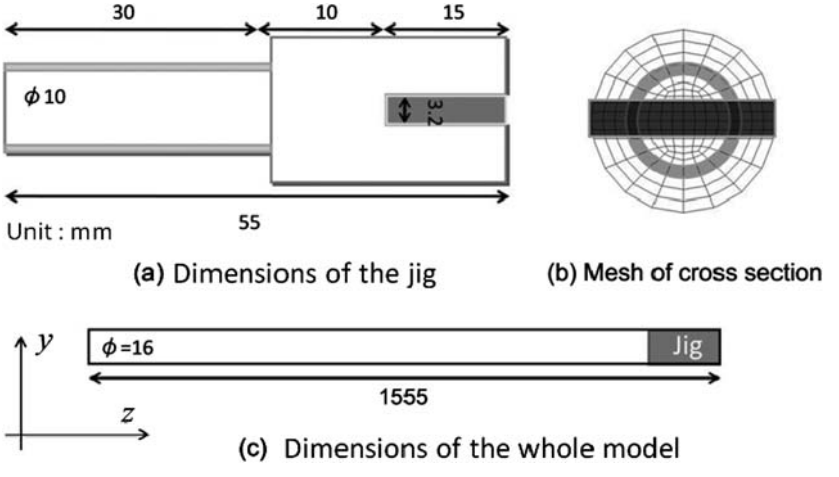

Figure 11. Numerical model of the jig and input bar.

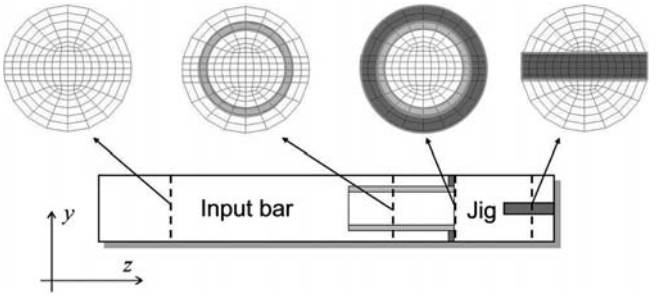

Figure 12. Configuration of the material properties at each cross section.

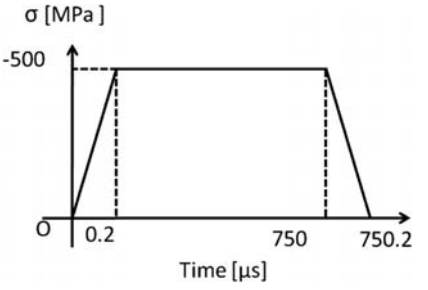

Figure 13. Loading condition for evaluating the effect of the jig with a slit and screw.

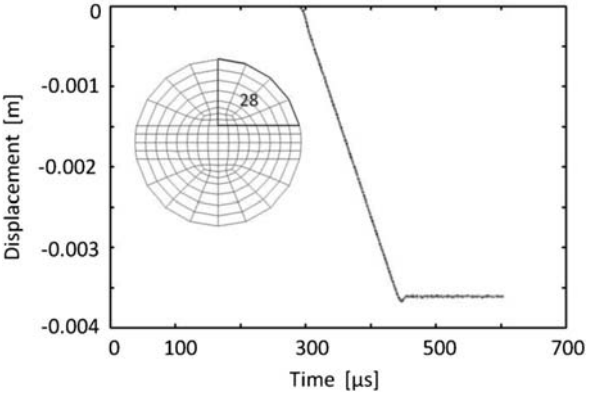

Figure 14. Simulated displacement at $x = 2320$ (left end of jig).

The displacements in the z direction were observed at $z = 1555$ mm. The displacements of the 28 elements encircled by the black line in Figure 14 were compared. The displacement transitions are represented by 28 lines. The good agreement between the 28 lines indicates that the right end of the jig can move uniformly. Therefore, it is found that the jig can apply an ideal one-dimensional displacement to a specimen.

5.2. Effect of duration time and fiber angle

The previous section shows that the jig with a slit and screw can apply a uniform displacement to a specimen. This section describes several numerical simulations of the SHPB using the jig to investigate the effect of the loading duration and the mismatch of the acoustic impedance between the steel input/output bars and the composite specimen on the stress–strain curve.

Figure 15 shows the numerical model of the SHPB considering the jig, input/output bars, and specimen. The width and effective length of the specimen were $w = 16$ mm and $l = 20$ mm, respectively. The composite specimen was modeled as an orthotropic elastic material, the material properties of which are listed in Table 2. The material constants of the input/output bars were as follows: the Young's modulus was 205 GPa, the Poisson's ratio was 0.25, and the mass density was 7800 kg/m^3. There were a total of 619,520 elements in the numerical model.

The transmitted wave ε_t was observed at $z = 2320$ mm, and the difference between the incident wave ε_i and the reflection wave ε_r was observed at $z = 500$ mm, as indicated by the black circles. The acoustic impedance mismatch is characterized by the angle θ between the fiber

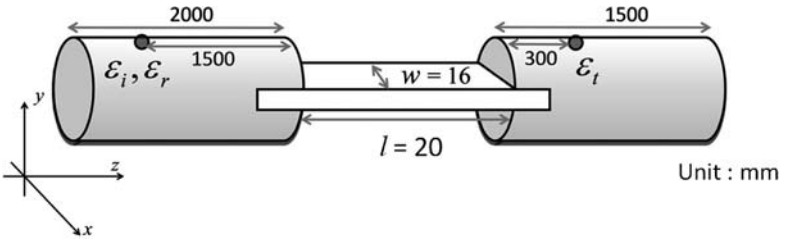

Figure 15. Dimensions of the SHPB model and observation points.

Table 2. Material properties of the composite specimen.

Young's modulus (GPa)	E_1	130.3
	E_2	9.5
	E_3	9.5
Shear modulus (GPa)	G_{12}	4.7
	G_{23}	3.2
	G_{31}	4.7
Poisson's ratio	v_{12}	0.34
	v_{23}	0.5
	v_{31}	0.03
Mass density (kg/m^3)	ρ	1800

direction and the wave propagation direction, which corresponds to the z direction in Figure 16. If the angle becomes larger, the mismatch in acoustic impedance increases. The duration time λ is characterized in Fig. 17. We assumed three different angles ($\theta = 0°$, 45°, and 90°) and used two different duration times ($\lambda = 20$ and 100 μs)

Figure 18 shows the obtained stress–strain curves for different combinations of angle θ and duration time λ. In the legend, 'SHPB' denotes that its curve is obtained by SHBP theory using Equations (2) and (3) from the simulation observations, and 'Specimen' denotes that its stress–strain curve is observed directly from the simulation using the specimen alone, where the observation point is at the center of the specimen. We assumed that the stress–strain curves denoted 'Specimen,' which are indicated by the solid lines in each graph, give the ideal material behavior.

For the duration time of $\lambda = 20$ μs, the stress–strain curves of 'SHPB' and 'Specimen' have similar trends for $\theta = 0°$; meanwhile, their trends have significant differences for $\theta = 90°$.

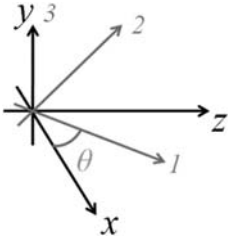

Figure 16. Definition of θ.

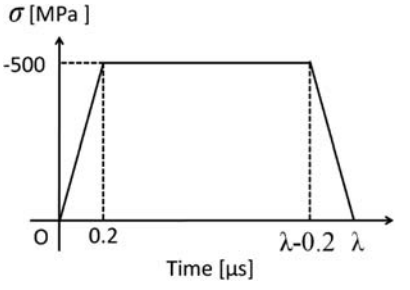

Figure 17. Duration time λ.

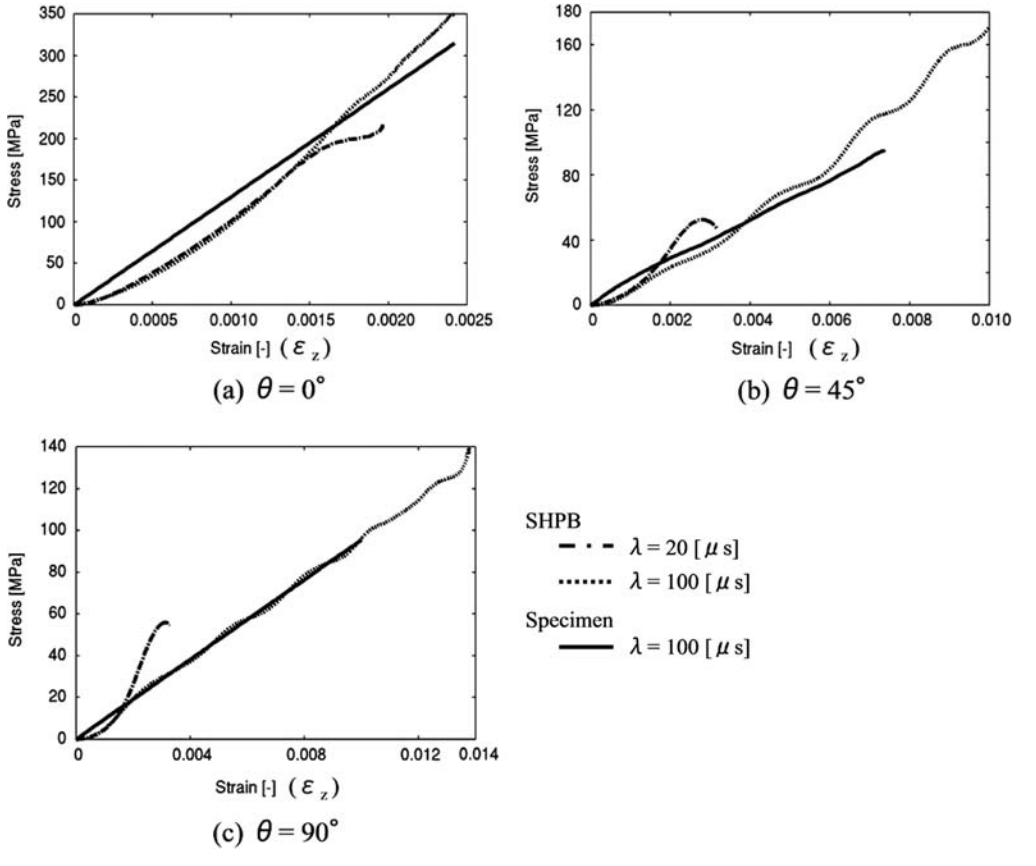

Figure 18. Stress–strain curves for different duration times and fiber angles.

For the duration time of $\lambda = 100\,\mu s$, the stress–strain curves for 'SHPB' and 'Specimen' have similar trends for both $\theta = 0°$ and $\theta = 90°$. These results indicate that if the acoustic impedance is smaller, a smaller duration time is sufficient for obtaining a reasonable stress–strain curve using the SHPB. Also, the results indicate the possibility of material characterization of the composite material by SHPB testing with a longer duration time if the acoustic mismatch is greater. For reference, the apparent Young's moduli for $\theta = 0°$, 45°, and 90° are 130, 12, and 9.5 GPa, respectively.

6. Conclusion

The present study proposed a simple numerical simulation technique for the SHPB and then investigated the experimental conditions for composite materials in a tensile-loading SHPB. The following issues were investigated through experiment and numerical simulation: (i) the effects of the cross section and acoustic mismatch between the jig with a slit and screw and the input/output bars on the loading condition and (ii) the effects of the duration time of the applied load and the acoustic impedance mismatch on the stress–strain curve obtained by SHPB testing. From the numerical simulation results, the following conclusions were found: (i) the proposed jig with a slit and screw can apply an ideal one-dimensional displacement to a specimen and (ii) the material characterization of a composite material by SHPB testing might be possible by optimizing a longer duration time if the acoustic mismatch is greater. In future work, we plan to propose criteria for determining a sufficient duration time.

References

[1] Taniguchi N, Nishiwaki T, Kawada H. Experimental characterization of dynamic tensile strength in unidirectional carbon/epoxy composites. Advanced Composite Materials. 2008;17:139–56.
[2] Gilat A, Goldberg RK, Roberts GD. Experimental study of strain-rate-dependent behavior of carbon/epoxy composite. Composite Science and Technology. 2002;62:1469–76.
[3] Melin LG, Asp LE. Effects of strain rate on transverse tension properties of a carbon/epoxy composite: studied by moiré photography. Composites: Part A. 1999;30:305–16.
[4] Shokrieh MM, Omidi MJ. Tension behavior of unidirectional glass/epoxy composites under different strain rates. Composite Structures. 2009;88:595–601.
[5] Harding J, Welsh LM. A tensile testing technique for fibre-reinforced composites at impact rates of strain. Journal of Material Science. 1983;18:1810–26.
[6] Taniguchi N, Nishiwaki T, Kawada H. Tensile strength of unidirectional CFRP laminate under high strain rate. Advanced Composite Materials. 2007;16:167–80.
[7] Onishi Y, Urago M, Amaya K, Aoki S. Efficient dynamic finite element method for 3D objects with uniform cross-section. International Journal for Numerical Methods in Engineering. 2005;63:1898–910.
[8] Suga K. Efficient dynamic simulation based on cross section of elastic object. Proceedings of 11th International Conference on the Mechanical Behavior of Materials, 2011. Available from: http://dx.doi.org/10.1016/j.proeng.2011.04.257